Strengthening of two-way reinforced concrete slabs with Textile Reinforced Mortars (TRM)*

Catherine Papanicolaou[1], Thanasis Triantafillou[2],
Ioannis Papantoniou[3] and Christos Balioukos[3]

Summary: An innovative strengthening technique is applied for the first time in this study to provide flexural strengthening in two-way reinforced concrete (RC) slabs supported on edge beams. The technique comprises external bonding of textiles on the tension face of RC slabs through the use of polymer-modified cement-based mortars. The textiles used in the experimental campaign comprised fabric meshes made of long stitch-bonded fibre rovings in two orthogonal directions. The specimens measured 2 x 2 m in plan and were supported on hinges at the corners. Three RC slabs strengthened by textile reinforced mortar (TRM) overlays and one control specimen were tested to failure. One specimen received one layer of carbon fibre textile, another one received two, whereas the third specimen was strengthened with three layers of glass fibre textile having the same axial rigidity (in both directions) with the single-layered carbon fibre textile. All specimens failed due to flexural punching. The load-carrying capacity of the strengthened slabs was increased by 26%, 53%, and 20% over that of the control specimen for slabs with one (carbon), two (carbon) and three (glass) textile layers, respectively. The strengthened slabs showed an increase in stiffness and energy absorption. The experimental results are compared with theoretical predictions based on existing models specifically developed for two-way slabs and the performance of the latter is evaluated. Based on the findings of this work the authors conclude that TRM overlays comprise a very promising solution for the strengthening of two-way RC slabs.

1 Introduction

Changes in a structure's usage, design errors and vernacular building practices (e.g. floating columns), introduction of more stringent design requirements, or strength reduction due to steel reinforcement corrosion are conditions that often call for retrofitting and strengthening of RC slabs. Flexural strengthening of RC slabs has received less attention both experimentally and analytically in comparison to flexural strengthening of RC beams. Moreover, the majority of relevant tests found in the literature feature flat slabs (i.e. lacking edge beams) which are simply supported around their perimeter (thus, allowing for edge uplift). This is not applicable for slabs supported on edge beams as the latter provide restraint against lateral movement resulting in compressive membrane action. Regardless of boundary conditions though, strengthening interventions based on the FRP technique have gained increasing popularity in recent years [e.g. externally bonded (EB) and/or mechanically fastened strips in two directions, EB bi- or multi-directional fabrics, near-surface mounted reinforcement]. This work provides additional support to the findings of previous investigations conducted by the authors [1], [2] indicating that the TRM technique provides a viable alternative to "classic" FRP interventions without compromising strength and ductility increase.

2 Experimental Program

2.1 Test specimens

The experimental program aimed to assess the effectiveness of TRM overlays as a measure of increasing the strength and deformation capacity of centrally loaded two-way RC slabs. To examine this, four specimens were tested under monotonic flexure. The specimens were square in plan with a side length of 2000 mm and a slab thickness of 120 mm. The slabs were uniformly cast with perimeter beams measuring 300 mm in height and 150 mm in width; therefore, the slab section of each specimen measured 1700×1700 mm in plan. One specimen was used as a control specimen, and the others were strengthened. Specimens' geometry is shown in Fig. 1.

All slabs were fabricated with identical structural steel reinforcement simulating lightly reinforced or, alternatively, moderately corroded slabs. Two welded wire fabrics (WWF) were used: the first comprised a T139 WWF [i.e. $100 \times 100\text{-W}13.8 \times \text{W}13.8$ $(\text{mm} \times \text{mm-mm}^2 \times \text{mm}^2)$] and was placed at the bottom (tension) surface of the slabs, whereas the second one was a T92 WWF [i.e $150 \times 150\text{-W}13.8 \times \text{W}13.8$ $(\text{mm} \times \text{mm-mm}^2 \times \text{mm}^2)$] and was placed at their top (compression) surface. The tensile reinforcement ratio was equal to 0.14%; the WWF placed at the compression side of the specimens was regarded as non-structural and was used to avoid cracking during handling and transportation of the slabs to the testing rig.

According to calculations, shear punching reinforcement was not necessary as tensile reinforcement yielding would occur at a load approximately equal to 70 kN (based on cross-

section analysis), which was lower than the estimated shear capacity of the slab owed solely to concrete contribution (equal to 81.5 kN – based on the formulation provided by EC2). Nevertheless, hoop reinforcement was placed around the perimeter of the loading area at the centre of the slabs in order to account for any calculation ambiguities and ensure tensile reinforcement yielding prior to punching failure, at least for the control specimen. The loading area measured 250×250 mm in plan. Two hoops (8 mm diameter stirrups measuring 500×70 mm) were placed adjacent and parallel to each side of the loading area at a distance equal to 125 mm and 250 mm from the centre point of the slabs for the first and the second hoop, respectively (Fig. 2). Hoops layout followed pertinent recommendations included in EC2.

The beams of the test specimens were heavily reinforced so that failure of the slabs would not be governed by failure of the supporting members. The longitudinal reinforcement consisted of four 12 mm diameter ribbed bars each one placed at the corners of the beam's cross-section. The bars of each beam were chamfered at the corners of the specimen at a radius of 120 mm and were spliced with contiguous ones over a length of 300 mm that provided adequate anchoring in the other two beams. Shear reinforcement was provided by 8 mm diameter closed stirrups with a spacing of 100 mm. The corners of the specimens, being the support areas, received additional reinforcement in the form of L-shaped rebars placed at cross-section's mid-height and extending by 300 mm in both beams of the joint. The minimum concrete cover in all parts of the specimens was maintained at 20 mm. Reinforcement details representative of all specimens are given in Fig. 3.
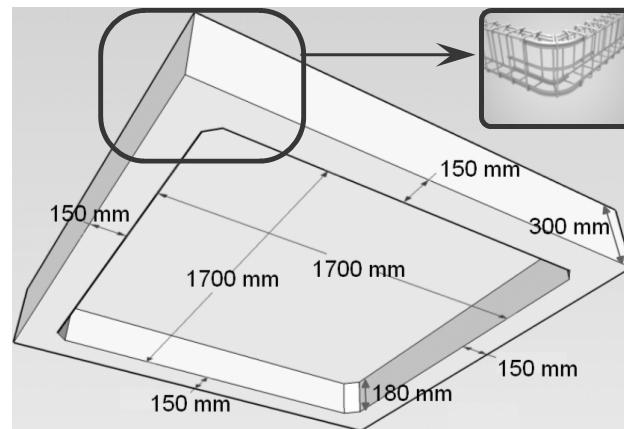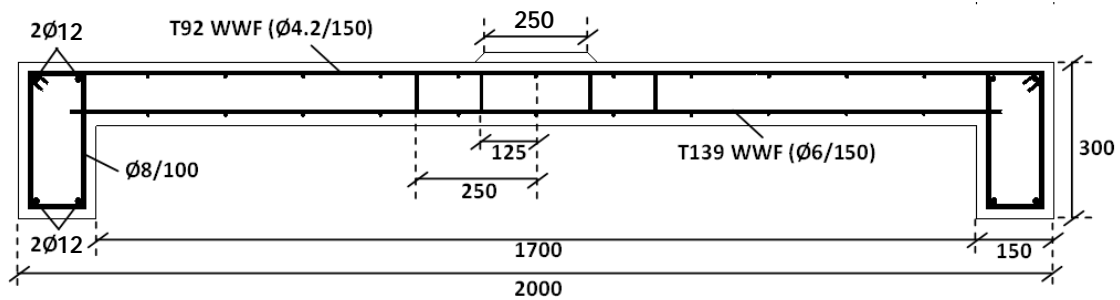

Fig. 4: Specimens' geometry

Fig. 5: Specimens' geometry

2.2 Materials, test set-up and instrumentation

All slabs were cast against stiff impermeable wooden formworks using the same concrete batch which was supplied by a local ready-mix plant. The 28-days' compressive strength measured using 150 mm cubes was found to be equal to 25.6 MPa, whereas the compressive strength at the day of specimens' testing was 31.2 MPa. The 28-days mean splitting tensile strength of the concrete mixture was equal to 3.3 MPa and was evaluated using three cylindrical specimens of 300 mm height and 150 mm diameter. All specimens (slabs, cubes and cylinders) were cured using wet burlaps for a period of ten days and then they were left outdoors until testing. Steel reinforcement properties were derived from three specimens per bar diameter. The results are given in Table 1. As shown in Table 2, the WWF used as tension reinforcement in the slabs was proved to be noticeably less deformable than the rest of the reinforcement used in the beams.

Table 3:   Reinforcement properties

Bar diameter [mm]	Yield stress [MPa]	Yield strain [%]	Ultimate strain [%]
12.0	559	0.28	14.6
8.0	573	0.29	11.5
4.2	645[†]	0.5[‡]	2.1

[†] Conventional yield stress at plastic strain = 0.2%;   [‡] Corresponding to the conventional yield stress

For the specimens receiving TRM overlays, commercial textiles with either high-strength carbon or E-glass fibre rovings arranged in two orthogonal directions were used. Both types of textiles shared the same geometry and comprised equal (but different between textiles) quantities of fibres in each direction. Each fibre roving (1650 TEX for carbon and 2400 TEX for E-glass, TEX being the linear roving weight in g/km) was 3 mm wide and the clear spacing between rovings was 7 mm. The weight of fibres in the textiles was 350 g/m^2 and 500

g/m^2 for the carbon fibre and the E-glass fibre textile, respectively (including the weight of the stitching thread). The nominal thickness of each layer (based on the equivalent smeared distribution of fibres) was 0.18 mm, for both types of textile. The guaranteed tensile strength of the fibres (as well as of the textile, when the nominal thickness is used) in each direction was taken from data sheets of the producer equal to 3500 MPa and 1750 MPa for carbon and E-glass fibres, respectively; the elastic modulus of the fibres was 220 GPa (carbon) and 72 GPa (E-glass). It becomes clear that in terms of axial rigidity (being equal to the product of textile layer thickness and textile modulus of elasticity, in either direction and per unit width) one layer of carbon fibre textile is equivalent to three layers of E-glass fibre textile.

The binding material comprised a commercial dry mortar blend, consisting of fine aggregates, cementitious materials and polymers (10%, by weight of the dry binder). The binder to water ratio was 4.3:1, by weight. The 28-days flexural and compressive strengths were 6.5 MPa and 24.6 MPa, respectively.

The application of the textile layers followed a procedure similar to the one applicable for conventional FRP interventions (Fig. 6a). First, the bottom surface of each slab (except of the control one) was ground even and brushed clean; then, dust and any loose particles were removed with high air pressure and the surface was dampened using a wet sponge. Upon completion of the preparatory works a layer of mortar was applied on the surface and the textile sheet was subsequently bonded by hand and roller pressure. Mortar was also applied in between layers (for multi-layered overlays), as well as on top of the last textile layer. Application of the mortar was made in approximately 2 mm thick layers with a smooth metal trowel. The textile was pressed slightly into the mortar, which protruded through all the perforations between fibre rovings. Of crucial importance in this method, as in the case of epoxy resins, was the application of each mortar layer while the previous one was still in a fresh state. Curing of the mortar was achieved in outdoor conditions.

Three specimens were strengthened in total, whereas one served as the control specimen (designated henceforth as "CON"). One specimen received one layer of carbon fibre textile (specimen 1C), another one received two (specimen 2C), whereas the third specimen was strengthened with three layers of E-glass fibre textile (specimen 3G) having the same axial rigidity (i.e. equal product of fibres' modulus of elasticity and textile thickness) with the single-layered carbon fibre textile (in both directions). These strengthening schemes were selected in this study so that they would provide useful insight to the effects of the fibre reinforcement ratio and the number of TRM layers (of equivalent axial rigidity).

Two- and three-layered strengthening schemes were realized with every subsequent layer being bonded in the transverse direction compared to the direction of application of the previous layer. In this way, the only unreinforced areas of the slabs were the four corners measuring 200x200 mm. In order to provide to specimen 1C anchoring conditions equivalent to those of the rest of the strengthened specimens, two strips of the same textile were added adjacent to the strengthening layer so that beam-to-beam coverage was also achieved in the

transverse direction; the overlapping between the strips and the central textile piece was equal to 130 mm (Fig. 7b).

All specimens were subjected to monotonic compressive loading at mid-span – in a displacement-control mode – using the stiff steel frame and support steelwork shown in Fig. 8c. The displacement was applied at a rate of 0.017 mm/sec, using a vertically positioned 500 kN MTS actuator of 250 mm stroke capacity. In order to avoid stress concentrations at the loaded area the piston's swivels acted against a 20 mm thick square steel plate with a side of 250 mm resting on a base projecting from the slab; the base (measuring 300x300x20 mm) consisted of a high strength cementitious mortar strengthened with a piece of T139 WWF. All specimens were simply supported at their corners on ball-bearing hinges (thus, they were free to rotate at these points).

Prior to concreting, four strain gauges were attached on the tensile reinforcement of each slab, one on each of the four wires comprising the central mesh. Displacements were monitored using eight rectilinear displacement transducers: seven were fixed on the bottom surface of each slab, in a cruciform configuration (a centrally placed one, four others along one direction and two more along the other, all at a spacing of 200 mm), whereas the eighth transducer was fixed at the top surface of the slabs close to their centre-point. Data from all transducers were recorded using a fully computerized data acquisition system. The resulting load–displacement curves were generated by the system in real time. The test was run in a fully computerized manner and was completed (manually terminated by returning the piston to zero position) after the ultimate capacity of the specimen was reached and a considerable load reduction was evidenced.
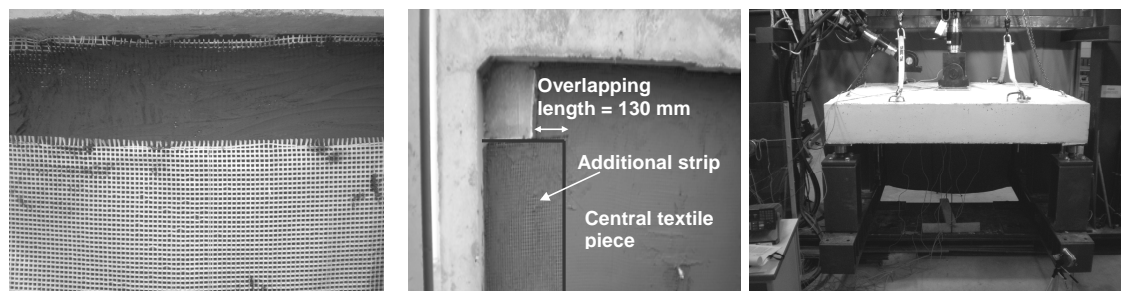
(a) Slab 3G: second layer of E-glass fibre textile in place (prior to pressing it into the fresh mortar) (b) Slab 1C: anchoring of the central textile piece (c) Test set-up

Fig. 9: Application details and test set-up

3 Test Results and Discussion

The load versus centre-point deflection (measured by the displacement transducer positioned at the soffit centre) for all specimens is shown in Fig. 10. Load values do not include the dead load of the slabs (approximately 17 kN) and deflection values do not include the dead load contribution as being negligible. Load versus strain of steel bars is presented in Fig. 11. Main experimental values (load and centre-point deflection) at critical points of the specimens' response (first crack, steel yielding, maximum and ultimate capacity) are presented in Table 4 and Table 5.

All specimens responded in a similar manner in terms of crack development and failure mode. In the uncracked stage – denoted by the first linear part of the load-deflection curves – the initial stiffness of all strengthened specimens was higher than the one of the control specimen. For all slabs first cracking due to flexure occurred – as expected – directly below the load application area and at approximately the same load value (Table 6); this is reflected on the load-deflection response at the point where the curves deviate from linearity and a marked reduction in stiffness is evident (note: at this point first cracking in both directions had occurred in a consecutive way).

With increasing imposed displacement more flexural cracks formed in both directions along the bars of the tensile steel reinforcement grid (this being more visible in the control specimen) and diagonal cracks were generated propagating from the centre of the specimens to the corners. As shown in Table 7, yielding of tensile reinforcement in both directions was delayed in all strengthened specimens (by more than approx. 30% in terms of yielding load in the direction along which yielding first occurred).

In addition to slab cracking both flexural and torsional cracks formed on all four beams of each specimen; torsion was the result of differences in rotation at the corners of the specimen at any given level of central deflection after first cracking. Crack patterns at failure for all specimens are given in Fig. 12. Among all strengthened specimens slab 2C exhibited a denser crack pattern. In all specimens, a nearly circular crack developed on the compression face just above the beam-slab connection plane, at approximately 70% of the load at failure, denoting slippage of the top welded wire fabric from the beams; in addition, cracks perpendicular to the diagonals of the slabs were developed in the vicinity of the supports owing to the in-plane restraint provided by the latter.
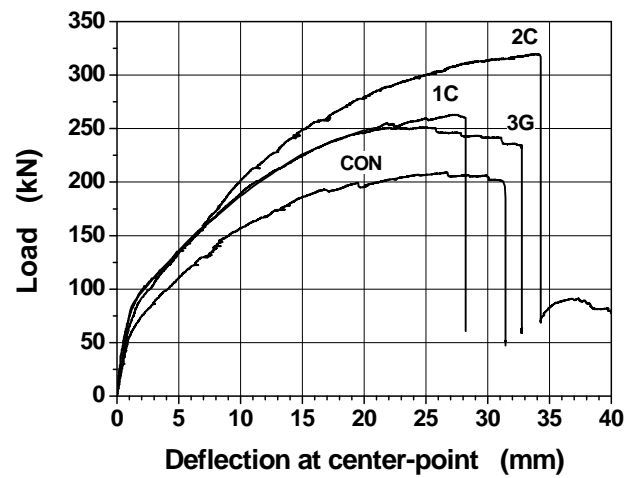
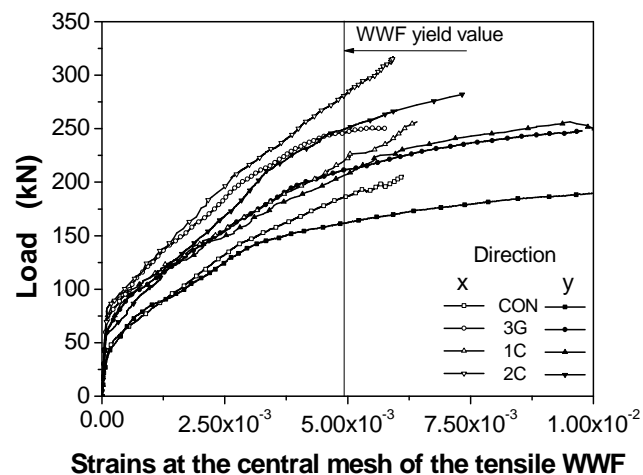**Fig. 13:** Load vs centre-point deflection curves

Fig. 14: Load vs measured reinforcement strains curves

The failure mechanism consisted of the sudden punching out of a pyramoid concrete plug at the centre of the slabs; the 300 mm square base comprised its top surface, whereas the bottom one formed an ellipsoid (common for relatively high ratios of slab span over thickness, equal to approx. 14 in this work). Punching was accompanied by immediate and significant drop in load. The punched concrete plug was steeper (in the narrower direction) in the control specimen in comparison to the strengthened ones. After failure occurred the flatness of the slabs was maintained outside the load application area. Failure is characterised as "flexural punch-

ing" since punching occurred shortly after yielding of the flexural reinforcement (in both directions) near the load application point (Fig. 15).

The increase in textile layers (1C to 2C) did not lead to an undesirable failure mode (debonding of the TRM overlays from the soffit - common for FRP strengthening). Furthermore, increasing the overlay thickness while keeping the same axial rigidity resulted in an almost identical response of specimens 1C and 3G; for the latter, premature failure in the form of inter-layer delamination was avoided (this was attributed to the high shear strength of the mortar and to the relatively short span of the slab). Stepwise load reduction following the achievement of maximum load-carrying capacity for specimen 3G denotes gradual fibre fracture, whereas the enhanced deformation capacity of this specimen (in relation to specimen 1C – d_u/d_{y1} ratio in Table 8 provides a measure of the specimens' deformation capacity) is the result of inter-laminar slippage. It is notable that the deformation capacities of specimens 1C and 2C are practically identical. The load-carrying capacity of the strengthened slabs was increased by 26%, 53%, and 20% over that of the control specimen for slabs 1C, 2C and 3G, respectively, as the external TRM reinforcement delayed tensile steel yielding.
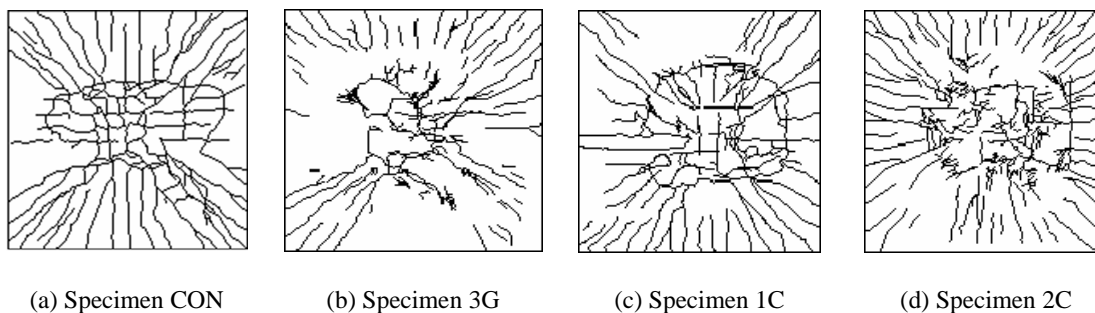

(a) Specimen CON   (b) Specimen 3G   (c) Specimen 1C   (d) Specimen 2C

Fig. 16: Crack patterns for all specimens

Table 9:   Experimental results at first crack and at steel yielding

Specimen	First crack		Yielding[†]			
	Load P_{cr} [kN]	Deflection d_{cr} [mm]	Load $P_{y,1}$ [kN]	Deflection $d_{y,1}$ [mm]	Load $P_{y,2}$ [kN]	Deflection $d_{y,2}$ [mm]
CON	54.0	0.93	161.4	10.7	185.5	14.9
3G	56.0	0.78	210.9	12.8	246.1	19.8
1C	54.8	0.68	206.3	12.4	219.5	14.1
2C	54.9	0.55	249.0	15.1	275.4	19.2

[†] Numeric subscript '1' denotes the direction along which steel yielding developed first; numeric subscript '2' denotes the direction along which steel yielding developed consecutively to '1'.

Table 10: Experimental results at maximum and at ultimate

| Specimen | Maximum | | Ultimate | | $\dfrac{d_u}{d_{y1}}$ | $\dfrac{P_{max} - P_{max\_CON}}{P_{max\_CON}}$ |
	Load P_{max} [kN]	Deflection d_{max} [mm]	Load P_u [kN]	Deflection d_u [mm]		
CON	209.0	26.6	196.1	31.4	2.93	-
3G	251.2	24.5	233.2	32.8	2.56	20.2%
1C	262.9	27.2	259.4	28.3	2.28	25.8%
2C	319.8	33.7	316.5	34.3	2.27	53.0%

4 Test Results Compared To Existing Formulations

Test results (maximum load) were compared to predictions provided by formulations proposed in the literature [3], [4], [5] and [8] [Eq. (1), (2), (3) and (4), respectively] in order to calculate ultimate strength at punching failure. In the first three formulations the flexural strength of the specimens was derived from two existing alternative relations based on the yield-line theory [6] and [7] [Eq. (5) and (6), respectively], whereas the moment resistance of the slabs was calculated through section analysis. The fourth formulation [Eq. (7)] comprised a simple model assuming that punching is a form of combined shearing and splitting under complex three dimensional stresses due to flexure/shear interaction. For this model the measured angle of the pyramoid concrete plug that was punched out from the slab at failure was equal to 31° (corresponding to the narrow side of the plug); this value agrees with the suggested value of θ in Eq. (8). Experimentally and analytically derived values of ultimate slabs' strengths are given in Table 11 (where $P_{max} \equiv V_u$).

$$V_u = \frac{15\left((1 - 0.075c/d)bd\sqrt{f_c}\right)}{1 + 5.25bd\sqrt{f_c}/V_{flex}} \tag{9}$$

$$V_u = \frac{0.8\left((1 + d/c)bd\sqrt{f_c}\right)}{1 + 0.433bd\sqrt{f_c}/V_{flex}} \tag{10}$$

$$V_u = \frac{2.24\left((1 - 0.075c/d)bdf_{ct,sp}\right)}{1 + 0.784bdf_{ct,sp}/V_{flex}} \tag{11}$$

$$V_u = \frac{2dx_f(c + 3d)\cot\theta f_{ct,sp}}{0.25d + x_f} \tag{12}$$

$$V_{flex} = 8m_u \left(\frac{1}{(1 - c/\ell)} - 3 + 2\sqrt{2} \right) \qquad (13)$$

$$V_{flex} = m_u \left(\frac{8c}{(\ell - c)} + 2\pi \right) \qquad (14)$$

with V_u failure load of slab (due to punching)

V_{flex} failure load of slab (due to flexure), in pounds for (15) & (16), in N for (17)

c max dimension of the load application area

d distance of tensile reinforcement from slab top

b perimeter of the load application area [c, d & b in inches for (18) & (19), in mm for (20), (21) & (22)]

x_f depth of compression zone in slab due to flexure (derived from section analysis)

θ angle of punched concrete plug (suggested value: 30°)

ℓ span of slab, in mm

m_u flexural moment capacity of slab (derived from section analysis), in Nmm/mm

f_c compressive strength of concrete, in psi for (23), in MPa for (24)

$f_{ct,sp}$ splitting tensile strength of concrete, in psi for (25), in MPa for (26).

Table 12:   Experimental and predicted maximum load

Specimen	$P_{max,test}$	$P_{max,(27)\_(28)}$	$P_{max,(29)\_(30)}$	$P_{max,(31)\_(32)}$	$P_{max,(33)\_(34)}$	$P_{max,(35)\_(36)}$	$P_{max,(37)\_(38)}$	$P_{max,(39)}$
CON	209.0	122	118	136	131	122	118	154
3G	251.2	301	276	335	328	307	301	258
1C	262.9	313	308	348	341	319	313	267
2C	319.8	373	368	414	409	382	377	323

5 Conclusions

In this study, the flexural response of two-way, simply supported, RC slabs strengthened with 0°/90° TRM overlays was experimentally investigated. Observed behaviour and test results

confirm that TRM overlays are successful in increasing the load-carrying capacity of flexure-critical RC slabs acting as external reinforcement with improved bonding conditions to the substrate. Load-carrying capacity increases with increasing fibre reinforcement ratio, overlays of equal axial rigidity per direction result in comparable increase in elements' ultimate strength, and inter-layer relative slippage in multi-layered systems seems to enhance the deformation capacity of the slabs. Although all strengthened specimens in this study failed due to flexural punching, the failure mode is likely to change into a brittle shear punching one should TRM overlays of higher axial rigidity be used. The predictions of ultimate strength from existing formulations based on yield line theory are very conservative for the unstrengthened slab; on the contrary, they are unsafe for the strengthened specimens tested in this study. Excellent agreement between test and analytical results was achieved when a simple existing model taking into account flexure/shear interaction was used to predict the post-yielding ultimate punching shear strength.

6 References

[1] TRIANTAFILLOU, T.C.; PAPANICOLAOU, C.G.: Shear strengthening of reinforced concrete members with textile reinforced mortar (TRM) jackets. *RILEM Materials and Structures* 39(1) (2006), pp. 85–93.

[2] BOURNAS, D.A.; LONTOU, P.V.; PAPANICOLAOU, C.G.; TRIANTAFILLOU, T.C.: Textile-Reinforced Mortar versus Fiber-Reinforced Polymer Confinement in Reinforced Concrete Columns. *ACI Structural Journal* 104(6) (2007), pp. 740-748.

[3] MOE, J.: Shearing Strength of Reinforced Concrete Slabs and Footings under Concentrated Loads. *Research and Development Laboratories Bulletin D47*, Portland Cement Association (PCA), (1961), Skokie, IL, USA.

[4] MOWRER, R.D.; VANDERBILT, M.D.: Shear strength of lightweight aggregate reinforced concrete flat plates. *ACI Structural Journal* 64(11) (1967), pp. 722–729.

[5] HOGNESTAD, E.; ELSTNER, R.C.; HANSON, J.A.: Shear Strength of Reinforced Structural Lightweight Aggregate Concrete Slabs. *Journal of American Concrete Institute* 61(6) (1964), pp. 643- 656.

[6] ELSTNER, R.C.; HOGNESTAD, E.: Shear Strengthening of Reinforced Concrete Slabs. *Journal of American Concrete Institute* 53(7) (1956), pp. 29–59.

[7] GESUND, H.: Design for Punching Strength of Slabs at Interior Columns. *Advances in Slab Technology*(1980), pp. 173-184.

[8] THEODORAKOPOULOS, D.D.; SWAMY, R.N.: Ultimate Punching Shear Strength Analysis of Slab-Column Connections. *Cement & Concrete Composites*, 24 (2002), pp. 509-521.